

Automatic Collision Avoidance Using Model-predictive Online Optimization

Moritz Werling and Darren Liccardo

Abstract—In many traffic emergency situations a collision cannot be prevented by braking alone. Therefore, we propose an obstacle avoidance algorithm that simultaneously optimizes steering and braking. As an emergency scenario approaches the driving limits, a strong nonlinear constraint between braking and cornering develops, suggesting the formulation of a nonlinear constrained online optimization. On this account the proposed algorithm embarks on the nonlinear model-predictive control (NMPC) paradigm, which is capable of solving the optimization problem online. The performance of the algorithm is demonstrated in a simulated pedestrian collision avoidance scenario.

I. INTRODUCTION

In recent years, there has been a strong increase in advanced driver assistance systems on the automotive market. Automatic emergency braking significantly reduces the threat of rear-end collisions as well as protects pedestrians from accidents [4]. However, in many real-world traffic situations, the remaining time to a collision is too short to sufficiently decrease high relative velocities to the obstacles. In these cases, a collision can only be prevented by additional steering intervention [9]. In this paper we focus on the planning of this evasive maneuver. Here, the challenges are

- the presence of moving obstacles,
- coupling effects between lateral and longitudinal vehicle dynamics,
- short planning cycles for a short response time, and
- minimization of the driver's irritation.

In this work, we approach these challenges with the application of nonlinear model-predictive control (NMPC) [8].

After an overview on related work in Sec. II, we introduce in Sec. III a simplified vehicle model, which also describes the kinematics of a reference curve. In Sec. IV we impose further constraints on this model in order to account for the physical limits of the vehicle and the desired avoidance direction. We then propose an objective function in Sec. V, which evaluates the obstacle avoidance trajectory. Section VI briefly describes the implementation of the algorithm, which will be evaluated in a simulated pedestrian scenario in Sec. VII. Finally, a short summary and an outlook are given in the concluding Sec. VIII.

M. Werling is with BMW Group Research and Technology, Hanauer Strasse 46, 80992 Munich, Germany, moritz.werling@bmw.de

D. Liccardo is with BMW Group Technology Office USA, 2606 Bayshore Parkway, Mountain View, CA 94043, USA, darren.liccardo@bmw.de

II. RELATED WORK

Model-predictive trajectory planning has been first proposed for aerial vehicles, such as in [12], and soon applied to vehicle applications, e.g. [11], [19], [10]. Recent work has been presented in [16], [3], [13], [15]. The application of NMPC to the problem of stabilizing a vehicle along a given trajectory can be found in [7], [13].

The main contribution of our work is the development of a trajectory planning algorithm for automatic collision avoidance amidst moving obstacles. As opposed to previous planning strategies, our algorithm pursues a combined optimization of braking and steering with consideration of nonlinear coupling effects between the longitudinal and lateral vehicle dynamics. That is, contrary to existing approaches, where braking plays a minor role during planning, we focus on the continuous transient between braking and swerving at the traction limits of the wheels. Moreover, the proposed strategy effectively leverages optimization constraints in order to avoid numerical convergence problems associated with local minima due to the presence of obstacles.

III. SYSTEM DYNAMICS

The essence of model-predictive control is to optimize a forecast of the system behavior. As this is accomplished with a system model, it is the most important element of a model-predictive controller [18]. However, for the sake of robustness, the proposed algorithm will not feed the optimized trajectory directly to the actuators. Instead, we follow the human strategy [17] and incorporate a fast compensatory feedback controller (cf. [16]), see Sec. VI. This facilitates the model-predictive optimization as a longer cycle time can be chosen without jeopardizing overall system stability. In addition, the incorporated prediction model can be designed in favor of a fast optimization process as long as the relevant vehicle properties are sufficiently accounted for.

With this in mind, we propose the first part of our prediction model,

$$\dot{x}_1 = v \cos \theta \quad (1)$$

$$\dot{x}_2 = v \sin \theta \quad (2)$$

$$\dot{\theta} = \frac{v}{l \left[1 + \left[\frac{v}{v_{ch}} \right]^2 \right]} \delta \quad (3)$$

$$\dot{\delta} = u_1 \quad (4)$$

$$\dot{v} = u_2. \quad (5)$$

As depicted in Fig. 1, x_1, x_2 and v represent the vehicle's reference position and velocity, respectively, θ denotes the course direction, and δ is the steering angle of the wheels. The steering rate as well as the time derivative of velocity serve as the system's inputs u_1 and u_2 . The model incorporates in (3) the steady state (yaw) dynamics [2] of a linear one-track model, whose sole parameter is the characteristic velocity

$$v_{ch} = \sqrt{\frac{l^2 c_f c_r}{m[c_r l_r - c_f l_f]}}, \quad (6)$$

which depends on the vehicular mass m , the cornering stiffness c_f and c_r of the front and rear wheels, the distances l_f and l_r between the front and rear axis to the center of gravity, as well as their sum l .

This model offers two major advantages over the regular one-track model. Firstly, it has no singularity at $v = 0$ and therefore allows for full stop braking. Secondly, the dynamics are particularly non-stiff, which permits a fairly large simulation step size of the ode-solver and thus speeds-up the optimization. However, in order not to overstrain the downstream feedback controller during extreme avoidance maneuvers, additional constraints have to be imposed on the trajectory, which will be defined in Sec. IV.

In preparation for effective computing of the objective function in Sec. V, we additionally model the dynamics of the vehicle's projection point onto a reference curve (e.g. the street center), depicted as the black dot on the dashed line in Fig. 1. The orientation θ_r , the signed distance d_r to the vehicle, and the covered arc length s_r represent the system states. Following differential geometry calculations [14], with $\kappa_r(s_r)$ being the arc-length parameterized curvature of the reference curve, the second part of our model reads

$$\dot{d}_r = v \sin(\theta - \theta_r) \quad (7)$$

$$\dot{\theta}_r = v \frac{\cos(\theta - \theta_r)}{1 - d_r \kappa_r(s_r)} \kappa_r(s_r) \quad (8)$$

$$\dot{s}_r = v \frac{\cos(\theta - \theta_r)}{1 - d_r \kappa_r(s_r)}. \quad (9)$$

Notice that the vehicle's trajectory can significantly deviate from the reference curve during obstacle avoidance (see later Sec. VII), therefore we do not linearize these dynamics. For arbitrarily shaped reference curves (e.g. s-shaped curves), we found this forward simulation method far more efficient than a numerical geometrical projection.

IV. PHYSICAL LIMITS AND MANEUVER CONSTRAINTS

In order to account for the limited wheel traction and actuator dynamics, as well as to force the vehicle to swerve around an obstacle on a given side, we additionally impose constraints on the trajectory.

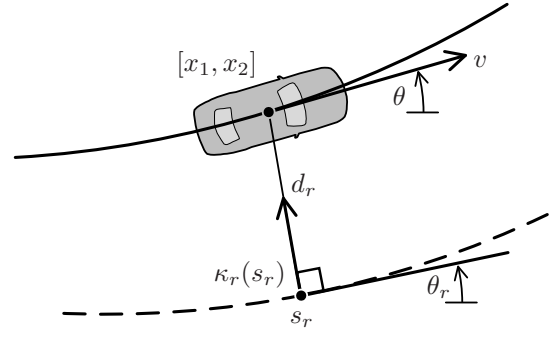


Fig. 1. System states of the simplified vehicle model and the reference curve

A. Steering, traction, and lane limits

The steering constraints are simply defined in box fashion,

$$u_1 \in [\dot{\delta}_{\min}, \dot{\delta}_{\max}] \quad (10)$$

$$\delta \in [\delta_{\min}, \delta_{\max}], \quad (11)$$

according to either the capability of the built-in power steering system or what can just be accepted by a driver.

Furthermore, it is reasonable from a safety point of view to model the road boundary to avoid collisions with fast oncoming traffic or occluded pedestrians on the side walk. These limits will also be enforced by box-constraints,

$$d_r \in [d_{r,\min}, d_{r,\max}]. \quad (12)$$

As the total frictional force between a single tire and the road surface cannot exceed a certain maximum value (the radius of the so-called *Kamm's circle*), the dynamics of the entire vehicle are similarly limited. In good accordance with measurements the vehicle acceleration vector $[a_n, a_t]^T := [v\dot{\theta}, u_2]^T$ has to stay within a centered ellipse given by the semi-axes c_n and c_t , see Fig. 2, and therefore

$$\left[\frac{a_t}{c_t}\right]^2 + \left[\frac{a_n}{c_n}\right]^2 \leq 1 \quad (13)$$

has to hold at all times. Notice that only the lower, dark-gray part of the traction potential in Fig. 2 is relevant to the addressed emergency maneuvers, so that we disregard the flattened top part related to the maximum engine torque.

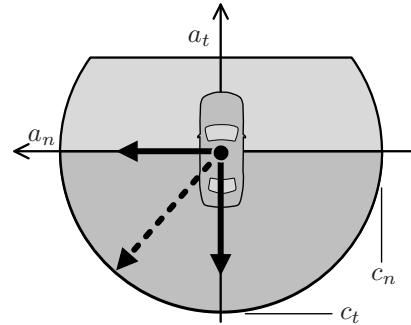


Fig. 2. Ellipse approximation of the combined lateral and longitudinal traction potential

B. Obstacles passing constraints

In the optimization we take obstacles into account by assigning costs to their vicinity, see Sec. V-B. This offers the major advantage over strict anti-collision constraints, in that the distances to the objects can be used as slack variables and reduced if required by the driving physics of an extreme scenario, see Sec. VII. However, as we do not want to leave the choice of the swerve direction to the numerical solver, we enforce the side to pass each obstacle by suitable constraints. That is, rather than letting the optimization itself converge into the left or right sided minimum of an obstacle, we constrain the side in advance, see Fig. 3.

We therefore introduce $\xi_m(\tau)$, $m \in 1 \dots M$, which denotes the vector from the (approximate) center of one of the M relevant, possibly moving, obstacles to the center of our evasive vehicle. In addition, we determine the point in time

$$t_{d_{\min},m} := \operatorname{argmin}_t d_m(\tau), \quad (14)$$

on the prediction horizon $\tau \in T_{\text{hor}}$

todo: tau und t beredenken

when the obstacle m has the smallest distance $d_m(\tau)$ to the ego vehicle (see also Sec. V-B below). With $\mathbf{n}(\tau)$ being the normal vector to the planned trajectory $[x_1(\tau), x_2(\tau)]^T$, see Fig. 3, we can now mathematically formulate the passing conditions using the scalar product: Passing on the left (right) side simply requires at $t_{d_{\min},m}$ that $\xi_m^T \mathbf{n} > 0$ ($\xi_m^T \mathbf{n} < 0$). As can be seen from the right side of the figure, these constraints also provide the correct behavior, even if the vehicle comes to standstill in front of the obstacle.

In order to avoid gradient-related convergence problems close to the center of an obstacle, we modify the above expression by some numerical clearance ξ_{num} . With $\gamma_m = -1$ for left and $\gamma_m = 1$ for right passing obstacle m , we finally get $\forall m = 1 \dots M$ that

$$g_{\text{pass},m}(\mathbf{x}; \gamma_m) := \gamma_m \xi_m^T(t_{d_{\min},m}) \mathbf{n}(t_{d_{\min},m}) + \xi_{\text{num}} \leq 0. \quad (15)$$

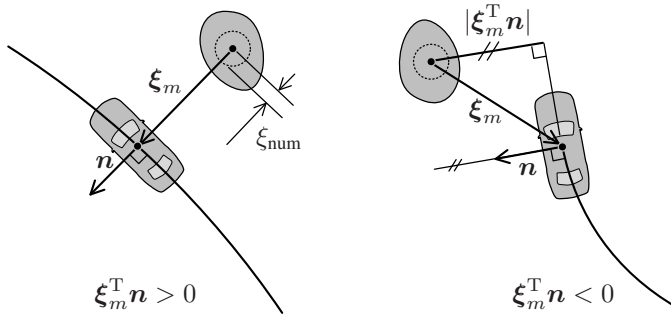


Fig. 3. Visualization of constraints controlling the passing side

V. COST FUNCTION

The optimization objective will be formulated as the minimization of a cost function. This cost function therefore serves as an inverse description of the ideal behavior. For evasive emergency maneuvers, this ideal behavior is characterized by a maximum reduction rate of potential energy, hence velocity. Furthermore, the vehicle should not get too close to any obstacle in order to account for perception errors and prediction uncertainties. And lastly, small deviations, both in position and orientation, from the reference curve minimize the possibility of secondary accidents with oncoming vehicles and help the driver to immediately regain control after automatic intervention. These verbal formulations will now be translated one after the other to mathematical expressions.

For the fastest possible velocity reduction, we not only require the acceleration vector to lie within the traction ellipse (13) but exactly on the boundary $[a_t/c_t]^2 + [a_n/c_n]^2 = 1$ at all times of the maneuver. The most efficient incorporation of this algebraic constraint in the optimization is solving for $a_t := \dot{v} = u_2$ and replacing u_2 in (5), which then reads

$$\dot{v} = -c_t \sqrt{1 - [v\dot{\theta}/c_n]^2} \quad (16)$$

We therefore neither need to account for the velocity reduction in the cost function nor treat u_2 as a separate variational function in the optimization process.

The remaining design objective will be covered in the following sections by splitting up the cost function J into a movement and an obstacle related term, that is

$$J(\mathbf{x}, u_1) = J_{\text{mov}}(\mathbf{x}, u_1) + J_{\text{obst}}(\mathbf{x}). \quad (17)$$

A. Movement costs

As for the lateral movement, the costs

$$J_{\text{mov}}(\mathbf{x}, u_1) = \int_t^{t+T_{\text{hor}}} \left\{ u_1^2 + \sum_{i \in \{v, a, j, \theta, \kappa\}} k_i \Delta_i^2(\mathbf{x}, u_1) \right\} d\tau \quad (18)$$

with

$$\Delta_v(\mathbf{x}) = v[\theta - \theta_r] \quad (19)$$

$$\Delta_a(\mathbf{x}) = v^2[\kappa - \kappa_r] \quad (20)$$

$$\Delta_j(\mathbf{x}, u_1) = v^2[\ddot{\kappa} - \ddot{\kappa}_r] \quad (21)$$

$$\Delta_\theta(\mathbf{x}) = \theta - \theta_r \quad (22)$$

$$\Delta_\kappa(\mathbf{x}) = \kappa - \kappa_r \quad (23)$$

and

$$\kappa := \frac{\delta}{l \left[1 + \left[\frac{v}{v_{\text{ch}}} \right]^2 \right]}, \quad \ddot{\kappa} := \frac{d\kappa}{d\delta} u_1, \quad \ddot{\kappa}_r := \frac{d\kappa_r}{ds} \dot{s}$$

meet the above requirements. Here, the dynamically motivated terms (19)-(21) penalize with $k_i > 0$ the proximate relative lateral velocity $\Delta_v \approx \dot{d}_r$, acceleration $\Delta_a \approx \ddot{d}_r$, and jerk $\Delta_j \approx \ddot{\ddot{d}}_r$. Due to the multiplication

with v these expressions dominate the trajectory costs at higher speeds and provide a certain *velocity invariance*: If the restrictions do not dominate the maneuver, the passengers will perceive the identical acceleration profile at 10 m/s as they will at 30 m/s . This in turn means, that no parameter adaption is required over the whole velocity range.

However, at low speeds shortly before the vehicle comes to standstill, these terms diminish. We therefore add the geometrically motivated terms (22) and (23), which in combination with the integral of u_1^2 in (18) provides for smooth stopping movements.

Note that unlike previous work, we omit a cost term for d_r . This is because we do not want the vehicle after the swerve to return to the road center on its own initiative by default, as undetected obstacles might be occluded by the primary obstacle.

B. Obstacle proximity costs

Costs in the vicinity of obstacles have been purposely omitted in the integral (18), as this leads to undesirable effects. For example, the faster the evasive vehicle drives past an obstacle, the smaller the time integrated costs become. Scaling the costs, e. g. by a factor of the difference velocity to an obstacle, results in other problems. We therefore consider the (predicted) minimum distance $d_{\min,m} := \min d_m$ of the vehicle's perimeter (see Fig. 4) to *each* object m over the *entire* optimization horizon. This leads to the weighted sum

$$J_{\text{obst}}(\mathbf{x}) = \sum_{m=1}^M k_{\text{obst},m} C_m(d_{\min,m}(\mathbf{x})). \quad (24)$$

Here, the utilized cost function given by

$$C_m(\cdot) = [\min([\cdot - d_{\text{infl},m}], 0)]^2 \quad (25)$$

with the zone of influence $d_{\text{infl},m}$, see Fig. 4, is chosen for four reasons: Firstly, in contrast to a linear cost increase, there is a distinct minimum of the overlayed costs between two close obstacles, and the shape around $d_{\text{infl},m}$ is sufficiently smooth for the optimization. Secondly, its computational effort is low. Thirdly, the costs are finite even for $d_{\min,m}$ smaller than zero. This is desirable because we prefer a collision mitigation to a collision free but non-feasible maneuver resulting from bad numerical convergence. Lastly, the vulnerability and prediction inaccuracy of an obstacle (both e. g. high for a pedestrian) can be, at least to some extent, accounted for by the weights $k_{\text{obst},m} > 0$ and the other parameter $d_{\text{infl},m}$.

This completes the optimization problem so that we can turn to the actual implementation in the following section.

VI. IMPLEMENTATION AND SIMULATION SETUP

For experimental validation of the proposed algorithm all required routines were developed in the C programming language embedded in the Matlab/Simulink simulation environment. The computations with a (simulated) sampling period of 0.1 s and an optimization horizon $T_{\text{hor}} = 2.0 \text{ s}$

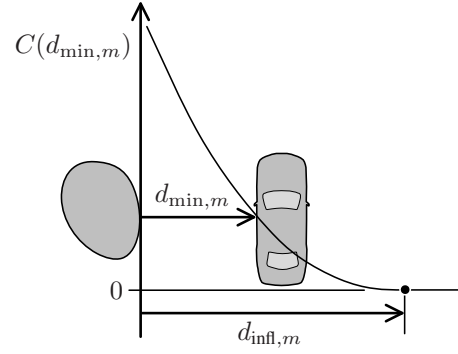


Fig. 4. Quadratic cost distribution in the vicinity of the obstacle m

are carried out by an i5-520M processor with 2.4 GHz . The optimization weightings (using SI-units) are chosen as $[k_v, k_a, k_j, k_\theta, k_\kappa] = [10^3, 10^2, 10^1, 10^2, 10^1, 10^0]$, the obstacle with $d_{\text{infl}} = 1.0 \text{ m}$ is accounted for by a factor of $k_{\text{obst}} = 10^5$, and the model is predicted with $v_{\text{ch}} = 50 \text{ m/s}$, $\dot{d}_{\text{max}} = -\dot{d}_{\text{min}} = 0.5 \text{ rad/s}$, $d_{\text{max}} = 2.0 \text{ m}$, $d_{\text{min}} = -1.5 \text{ m}$, $c_n = c_t = 8.0 \text{ m/s}^2$. The trajectory is passed to an i/o-linearizing feedback controller, which runs with a (simulated) cycle time of 0.01 s and feeds its control signals to the actuators of a simulated two-track vehicle. Besides sensor noise, also the dynamic loads, saturations as well as other nonlinear coupling effects of the wheels are modeled.

As the car can travel a considerable distance during a fraction of a second, the computation time of the optimization step cannot be neglected. We therefore utilize a *delay compensation by prediction* [6]. Furthermore, as we replaced u_2 by (16), we only need to parameterize the input u_1 , which we do by a piecewise constant control profile [1]. Due to the good nature (system stability) of the proposed model, the nonlinear-optimization problem can be implemented in a sequential fashion (single shooting, [6]) using the simple first-order Runge-Kutta method with a step size of 0.02 s . The minimization problem itself is solved by a standard sequential quadratic program (SQP) speeded up by a *real-time iteration* scheme [5].

VII. RESULTS

The top views of the simulation results are depicted by Fig. 5 through Fig. 7. Here, the optimized trajectory $[x_1, x_2]^T$ is represented by time-equidistant interconnected dots, the circle represents a pedestrian and the thick solid line its prediction on T_{hor} . On both sides of the vehicle the dashed lines mark the road boundaries, whereas the dash-dotted line serves as the reference curve.

Right below, the optimized input signal u_1 , the predicted steering angle δ , and velocity v are shown as time plots. Furthermore, in the lower left of each figure, the planned trajectory is projected into the acceleration plane $[a_n, a_t]$ within the 1.0 g -friction circle drawn in black.

In addition, the black arrow represents the desired acceleration vector forwarded to the feedback controller,

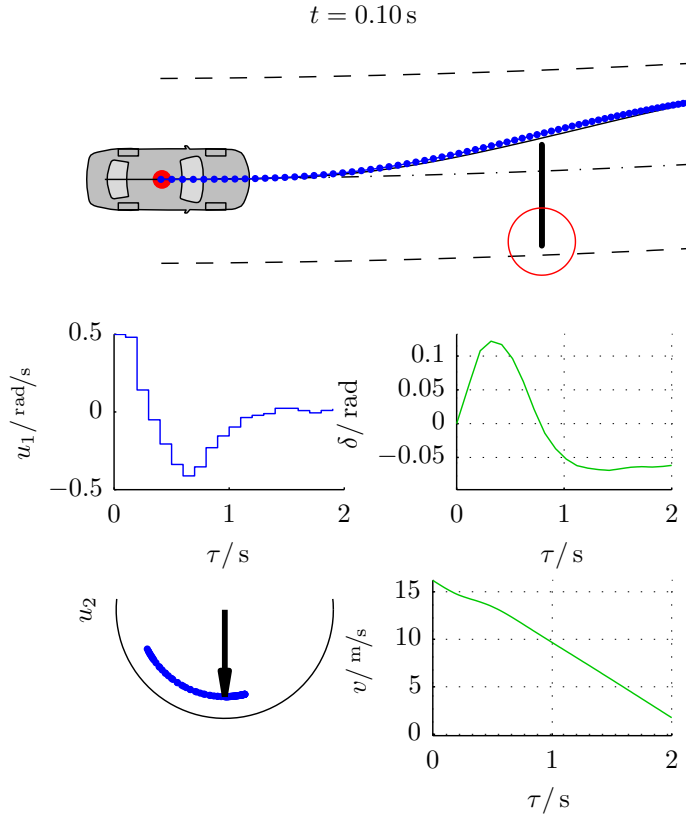


Fig. 5. Vehicle initiating collision avoidance maneuver

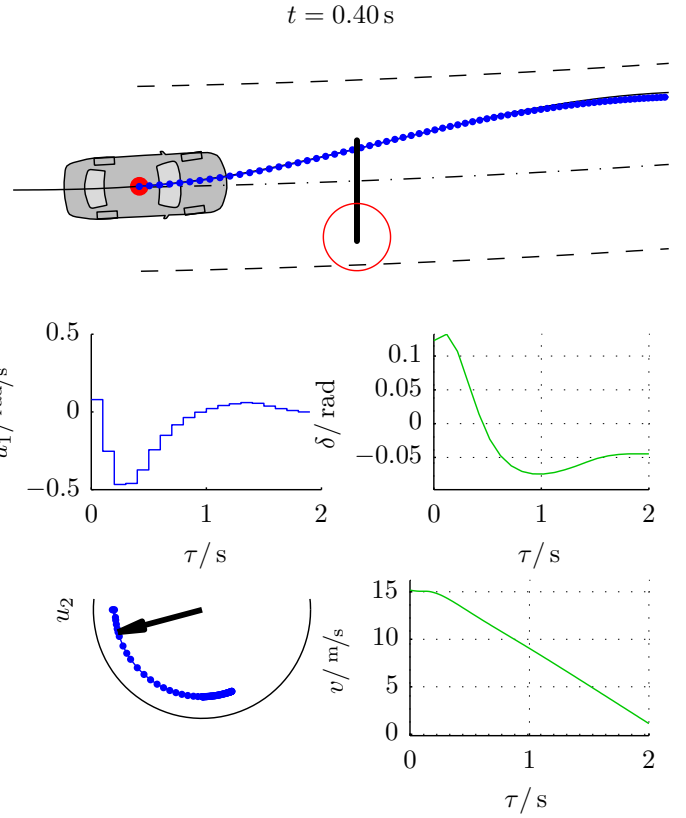


Fig. 6. Point in time with high lateral acceleration and low deceleration
 $t = 0.70$ s

whose a_t -component is the second system input u_2 . These three depicted points in time are also marked as vertical, dashed lines in Fig. 8, which shows the resulting closed-loop time signals of the steering angle δ_c and the velocity v_c of the simulated car. Below can be found the desired acceleration values a_{td}, a_{nd} commanded to the feedback controller and the actual measurements a_t, a_n .

At simulation start, the vehicle travels through a slight left curve with $v = 17.0$ m/s, when a pedestrian is detected on the right side of the lane. Its predicted trajectory activates the collision avoidance system, which initiates the combined braking and steering with the inherent delay of one cycle, see Fig. 5 and Fig. 8.

The underlying feedback controller instantly follows the optimized acceleration profile, see Fig. 8, so that approximately three planning cycles later the maximum lateral acceleration is reached, see acceleration arrow in Fig. 6. At this time the constraints therefore require reduced braking, which results in the dent of the velocity down-ramp shown to the right.

Another three cycles later the vehicle gets the closest to the obstacle, see Fig. 7, when the counter steering has already been initiated in order not to leave the given lane boundaries.

At $t \approx 2.5$ s the vehicle comes to a full stop and the experiment ends. Notice that the driven trajectory drawn in solid black in the top views, does not significantly deviate from the planned trajectory in the first cycle, see Fig. 5.

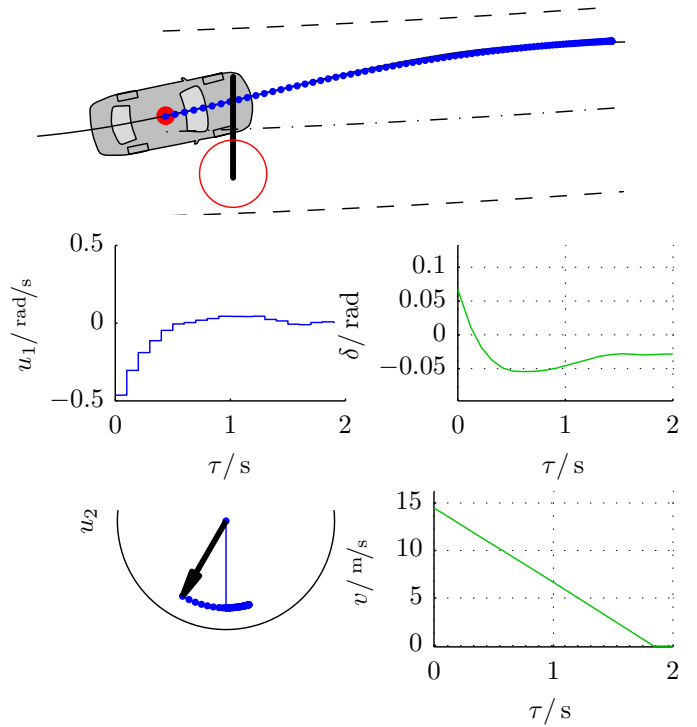


Fig. 7. Point in time when the obstacle is the closest

VIII. CONCLUSION AND FUTURE WORK

With an active steering system the gained degree of freedom has the high potential to safely handle situations

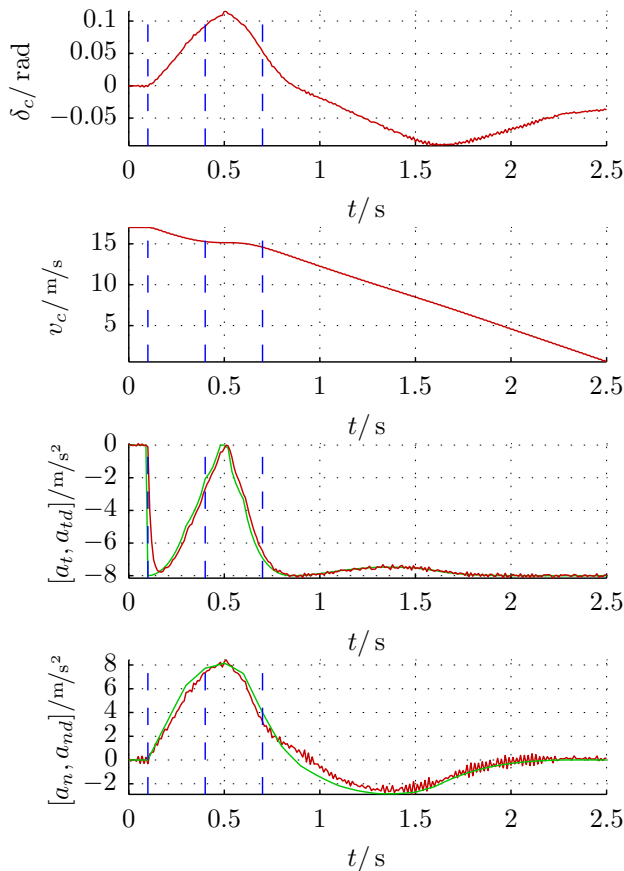


Fig. 8. Time signals of car and underlying feedback controller

where braking alone cannot prevent a collision. We therefore derived a planning strategy in the NMPC framework. In doing so, the special requirements of the application are accounted for by a simple, numerically efficient, and yet sufficiently accurate vehicle model. This model is subject to acceleration constraints limiting the combined braking and cornering wheel forces. Additional constraints factor in the steering dynamics, the lane width, and the desired swerving direction. Due to a thoughtfully chosen cost function the optimized trajectory compromises about steering effort (smooth movements) and the safe clearance to obstacles, which was demonstrated in a realistic simulation.

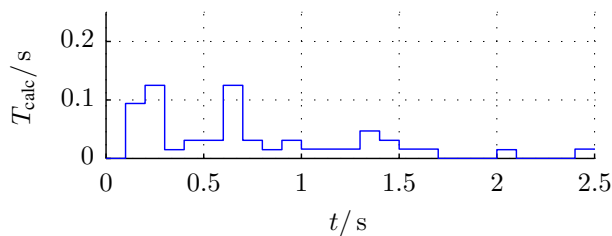


Fig. 9. Calculation time of SQP-optimization on a 2.4 GHz processor

Future research will focus on three things: 1) Porting the proposed setup from the simulation to a close-to-production real-time environment on a test vehicle equipped with all

required sensors. Considering the current calculation time of each planning cycle on the utilized comparably powerful processor, see Fig. 9, the real-time environment will require a considerably optimized implementation. 2) A substantiated stability analysis. 3) An improved low-level feedback controller enabling the full 1.0 g acceleration potential.

REFERENCES

- [1] M. Alami, A. Murilo, R. Amari, P. Tona, R. Fürhapter, and P. Ortner. On the use of parameterized nmmpc in real-time automotive control. *Automotive Model Predictive Control*, pages 139–149, 2010.
- [2] R.W. Allen, T.J. Rosenthal, and H.T. Szostak. Steady state and transient analysis of ground vehicle handling. Technical Report SAE No. 870495, Society of Automotive Engineers, 1987.
- [3] S.J. Anderson, S.C. Peters, T.E. Pilutti, and K. Iagnemma. An optimal-control-based framework for trajectory planning, threat assessment, and semi-autonomous control of passenger vehicles in hazard avoidance scenarios. *International Journal of Vehicle Autonomous Systems*, 8(2):190–216, 2010.
- [4] J. Breuer, S. Gleissner, A. Faulhaber, and P. Frank. Real world safety benefits of brake assistance systems. *Innovations for safety: Opportunities and challenges*, 2007.
- [5] M. Diehl, H.G. Bock, and J.P. Schlöder. A real-time iteration scheme for nonlinear optimization in optimal feedback control. *SIAM Journal on Control and Optimization*, 43(5):1714–1736, 2005.
- [6] M. Diehl, H. J. Ferreau, and N. Haverbeke. Efficient numerical methods for nonlinear mpc and moving horizon estimation. In Lalo Magni, Davide Martino Raimondo, and Frank Allgöwer, editors, *Nonlinear model predictive control*, pages 391–417. Springer, Berlin, 2009.
- [7] P. Falcone, F. Borrelli, J. Asgari, H. E. Tseng, and D. Hrovat. Predictive active steering control for autonomous vehicle systems. *Control Systems Technology, IEEE Transactions on*, 15(3):566–580, 2007.
- [8] R. Findeisen, L. Imsland, F. Allgöwer, and B.A. Foss. State and output feedback nonlinear model predictive control: An overview. *European journal of control*, 9(2-3):190–206, 2003.
- [9] Y. Hattori, E. Ono, and S. Hosoe. Optimum vehicle trajectory control for obstacle avoidance problem. *IEEE/ASME Transactions on Mechatronics*, 11(5):507–512, 2006.
- [10] T. Howard, C. Green, and A. Kelly. Receding horizon model-predictive control for mobile robot navigation of intricate paths. In *Field and Service Robotics*, pages 69–78. Springer, 2010.
- [11] A. Kelly and B. Nagy. Reactive nonholonomic trajectory generation via parametric optimal control. *The International Journal of Robotics Research*, 22(7-8):583–601, 2003.
- [12] H. Jin Kim, David H. Shim, and Shankar Sastry. Nonlinear model predictive tracking control for rotorcraft-based unmanned aerial vehicles. In *Proceedings of the 2002 American Control Conference*, pages 3576–3581, 2002.
- [13] Cunjia Liu, Wen-Hua Chen, and J. Andrews. Optimisation based control framework for autonomous vehicles: Algorithm and experiment. In *2010 International Conference on Mechatronics and Automation (ICMA)*, pages 1030–1035, 2010.
- [14] P. Morin and C. Samson. *Springer Handbook of Robotics*, chapter Motion control of wheeled mobile robots, pages 799–826. Springer, 2008.
- [15] M. Nanao and T. Ohtsuka. Vehicle dynamics control for collision avoidance considering physical limitations. In *SICE Annual Conference (SICE)*, pages 688–693. IEEE, 2011.
- [16] J.M. Park, D.W. Kim, Y.S. Yoon, H.J. Kim, and K.S. Yi. Obstacle avoidance of autonomous vehicles based on model predictive control. *Proceedings of the Institution of Mechanical Engineers, Part D: Journal of Automobile Engineering*, 223(12):1499–1516, 2009.
- [17] G. Prokop. Modeling human vehicle driving by model predictive online optimization. *Vehicle System Dynamics*, 35(1):19–53, 2001.
- [18] J.B. Rawlings. Tutorial overview of model predictive control. *Control Systems, IEEE*, 20(3):38–52, 2000.
- [19] C. Urmson, J. Anhalt, D. Bagnell, C. Baker, R. Bittner, MN Clark, J. Dolan, D. Duggins, T. Galatali, C. Geyer, et al. Autonomous driving in urban environments: Boss and the urban challenge. *Journal of Field Robotics*, 25(8), 2008.